Flow, Turbulence and Combustion (2026) 116:3
https://doi.org/10.1007/s10494-025-00703-1

RESEARCH

Flame Stabilisation Mechanism for Single and Multiple Jets in Cross-flow Using the Conditional Moment Closure

H. S. A. M. Awad[1] · P. Rajendram Soundararajan[2] · S. Gkantonas[1] · E. Mastorakos[1]

Received: 18 August 2025 / Accepted: 31 October 2025 / Published online: 24 November 2025

Abstract
The flame stabilisation mechanism for single and multiple reacting jets in cross-flow has been investigated using Large Eddy Simulation (LES) with the Conditional Moment Closure (CMC) as the sub-grid combustion model and a detailed chemical mechanism for pure hydrogen fuel. It has been found that a single jet in cross-flow (SJICF) has higher jet penetration depth compared to multiple jets in cross-flow (MJICF). This behaviour is attributed to the proximity of the counter-rotating vortex pairs of the three jets, which induces a downward negative velocity component, thereby influencing the jet stem. The flame stabilisation mechanism has been investigated using the budget of individual terms in the CMC equation. The CMC budget analysis reveals that upstream of the reactive zone, a premixed flame structure is observed with a convection-diffusion balance, whereas further downstream, a non-premixed flame structure prevails with a balance between micromixing and chemical reactions.

Keywords Flame stabilisation · Jet in cross-flow (JICF) · Conditional moment closure (CMC) · Large eddy simulation (LES)

1 Introduction

The use of hydrogen as an energy carrier remains important for the global reduction of greenhouse gases emitted from the energy sector. However, the use of hydrogen is not straightforward due to its high adiabatic flame temperature, which results in a high production of NOx emissions. Also, hydrogen is highly susceptible to flashback due to its high burning velocity. Thus, an effective mixing of fuel and air remains imperative to overcome the above-mentioned issues. An effective way to enhance the mixing between fuel and air is to inject the fuel perpendicularly into a cross-flow of air. This configuration is commonly

✉ H. S. A. M. Awad
hsama2@cam.ac.uk

[1] Department of Engineering, University of Cambridge, Cambridge CB2 1PZ, UK

[2] Department of Aeronautics & Astronautics, University of Southampton, Southampton SO16 7QF, UK

known as transverse jets or jet in cross-flow (JICF), where mixing is drastically enhanced due to the complex flow features accompanied by various flow structures such the Counter-Rotating Vortex Pairs (CVPs), Shear layer Vortices (SLVs), wake vortices and horseshoe vortices (Karagozian 2010). Due to its interesting mixing features, JICF has been used in various industrial applications such as turbine blade film cooling, fuel injection in combustion systems and combustion dilution in Rich-Quench-Lean combustors (Karagozian 2010; Awad et al. 2025a).

The JICF configuration has been investigated experimentally (Kamotani and Greber 1974; Kadota et al. 1990; Kelso et al. 1996; Hesselbrink and Mungal 1996; Steinberg et al. 2013; Huang and Wang 1999; Saini et al. 2021) and numerically (Yao et al. 2006; Kolla et al. 2012; Grout et al. 2011, 2012; Chan and Ihme 2013; Muralidharan and Menon 2014; Gkantonas and Mastorakos 2023) under both reacting and non-reacting conditions. Reacting investigations mainly focus on providing a more physical understanding of the flame stabilisation mechanism and the influence of heat release rate (HRR) on the flow field. Experimental investigation in reacting jet in cross-flow (RJICF) suggests that the flame base might be stabilised via partially premixed flame propagation (Hesselbrink and Mungal 1996). One of the important parameters that can influence flame stabilisation is the momentum flux ratio, which is defined as the momentum ratio J between the transverse jet and the cross-flow, and it is given as (Huang and Wang 1999):

$$J = \rho_j U_j^2 / \rho_\infty U_\infty^2 \tag{1}$$

where ρ_j and U_j are the density and velocity of the jet, and ρ_∞ and U_∞ are the density and velocity of the cross-flow. Different experimental investigations studied the influence of J on flame stabilisation (Steinberg et al. 2013; Huang and Wang 1999). For example, Steinberg et al. (2013) investigated hydrogen flames in RJICF under different J and observed two flame branches, one stabilising on the lee side and the other remaining lifted on the windward side of the flame. They also observed a more stable lee-side stabilisation as J increased. Saini et al. (2021) investigated the flame stabilisation characteristics in hydrogen-enriched natural gas, and it was found that as the hydrogen percentage increases the flame stabilises at both the windward and leeward side, whereas, at the low hydrogen percentage, the flame remains only anchored on the leeward side. The flame stabilisation mechanism in RJICF has also been investigated numerically using direct numerical simulations (DNS) and large eddy simulations (LES). DNS investigations for RJICF suggest that the flame is stabilised via partially premixed flame propagation in the vicinity of stochiometric mixture fractions and low-velocity magnitude (Kolla et al. 2012; Grout et al. 2011, 2012). Grout et al. (2012) conducted a DNS study to investigate nitrogen-diluted hydrogen RJICF and observed premixed-like flame characteristics near the stabilisation location. Chan and Ihme (2013) investigated hydrogen flames in RJICF using LES with a steady flamelet combustion mode. Their simulation overpredicted the stabilisation point and ignition onset, suggesting an extension of the flamelet formulation for a better prediction of RJICF. Muralidaran and Menon (2014) also used LES to investigate the stabilisation mechanism of nitrogen-diluted hydrogen RJICF and it was observed that flame anchoring is achieved through partial premixing.

Most of the above-mentioned investigations are based on a single jet in cross-flow (SJICF). However, practical applications may use multiple jets in cross-flow in close vicin-

ity (MJICF). Investigating MJICF may involve flame-flame interaction, which can affect the consumption speed (Im and Chen 2002), flame topology (Abo-Amsha et al. 2024) and flame surface area (Chen et al. 1999). Thus, it remains important to investigate the flame stabilisation mechanism in MJICF. The present research focuses on investigating the stabilisation mechanism for SJICF and MJICF using LES with the Conditional Moment Closure (CMC) as sub grid combustion model, which has been developed independently by Bilger (1993) and Klimenko (1990). The CMC model solves the conditionally averaged transport equations for all reactive scalars with respect to the mixture fraction as the conditioning variable. This allows direct evaluation of the local balance between convection, diffusion, chemical reaction, and micromixing in mixture-fraction space while incorporating detailed finite-rate chemistry at reduced computational cost. Unlike flamelet-type approaches, CMC does not assume functional dependence on mixture fraction, thereby enabling the description of non-steady behaviours including local extinction, reignition, and flame stabilization. CMC has been successfully applied in several studies to investigate lift-off and stabilization mechanisms in turbulent jet flames (e.g., Kim and Mastorakos 2005; Patwardhan et al. 2009; Navarro-Martinez and Kronenburg 2011) and transient events such as ignition and extinction (Zhang et al. 2015; Zhang and Mastorakos 2016; Awad et al. 2025b). Thus, the main objective of the current analysis is (1) to conduct an LES-CMC simulation for hydrogen RJICF, and (2) to investigate the flame stabilisation mechanism for SJICF and MJICF. The present paper is structured as follows. First, the governing equations are described. This is followed by a discussion of the experimental setup and numerical approaches. Then the results are discussed and finally, the main conclusions are summarised.

2 Methods

2.1 Governing Equations

The LES-CMC equation for the conditionally filtered mass fraction of a generic species, $Q_\alpha = \widetilde{Y_\alpha|\eta}$, is given as (Klimenko and Bilger 1999; Awad et al. 2025b):

$$\frac{\partial Q_\alpha}{\partial t} + \frac{\partial}{\partial x_i}\left(Q_\alpha \ \widetilde{u_i|\eta}\right) - Q_\alpha \frac{\partial}{\partial x_i}\left(\widetilde{u_i|\eta}\right) = \widetilde{N|\eta} \ \frac{\partial^2 Q_\alpha}{\partial \eta^2} + \widetilde{\dot{\omega}_\alpha|\eta} + e_\alpha \tag{2}$$

For the conditional enthalpy $Q_\alpha = \widetilde{h|\eta}$, the governing equation is given as (Klimenko and Bilger 1999; Awad et al. 2025b):

$$\frac{\partial Q_h}{\partial t} + \frac{\partial}{\partial x_i}\left(Q_h \ \widetilde{u_i|\eta}\right) - Q_h \frac{\partial}{\partial x_i}\left(\widetilde{u_i|\eta}\right) = \widetilde{N|\eta} \ \frac{\partial^2 Q_h}{\partial \eta^2} + e_h \tag{3}$$

where η is the sample space variable of the mixture fraction (ξ). The first from the left-hand-side of Eq. 2 is the unsteady term, which represent the temporal change of the conditionally average mass fraction. The second term is convective and it accounts for the transport of the conditional scalar by the conditionally averaged velocity field, and the third term accounts for the effect of dilatation term on the conditional scalar. The three terms from the right-hand side are the micromixing term, which consider the effect of molecular

diffusion, the conditional chemical source term $\widetilde{\dot{\omega}_\alpha|\eta}$, which is closed using first-order closure, and the turbulent diffusion term, which account for the sub-grid scale conditional scalar flux. $\widetilde{u_i|\eta}$ is the conditional velocity and it is closed using the local filtered velocity. $\widetilde{N|\eta}$ is the conditional scalar dissipation rate (SDR), which is closed using the Amplitude Mapping Closure (AMC) model as follows (O'Brien and Jiang 1991; Awad et al. 2025b):

$$\widetilde{N|\eta} = N_0 G(\eta) \tag{4}$$

with $G(\eta)$ being a bell-shaped function and N_0 is a scaling factor given as O'Brien and Jiang 1991; Awad et al. 2025b):

$$N_0 = \frac{\widetilde{N}}{\int_0^1 G(\eta)\,\widetilde{P}(\eta)\,d\eta} \tag{5}$$

where $\widetilde{N}$ is the filtered SDR given as (Foale 2022; Awad et al. 2025b):

$$\widetilde{N} = \widetilde{N}_{res} + \widetilde{N}_{sgs} = D\left(\frac{\partial \widetilde{\xi}}{\partial x_i}\right)^2 + \frac{C_N \mu_t \widetilde{\xi''^2}}{2\bar{\rho}\,\Delta^2} \tag{6}$$

where Δ is the filter width, C_N is a model constant, μ_t is the sub-grid scale turbulent viscosity and $D = \mu / \left(\bar{\rho}\,Sc\right)$ is the molecular diffusivity. The $\widetilde{\xi''^2}$ is the mixture fraction sub-grid scale variance and it is solved using a transport equation following (Foale 2022; Awad et al. 2025b). e_α represents the effect of sub-grid scales and is closed using the gradient assumption following (Foale 2022; Awad et al. 2025b):

$$e_\alpha = \frac{1}{\bar{\rho}\,\widetilde{P}(\eta)} \frac{\partial}{\partial x_i}\left[D_T \frac{\partial Q_\alpha}{\partial x_i}\right] \tag{7}$$

where D_T is the turbulent diffusivity, which is assumed equal for all species and a similar expression as Eq. 7 is used for e_h closure. Note that we have here assumed adiabatic conditions so no heat loss terms appear in Eq. 7. The LES-filtered unconditional quantities are obtained from the conditional by integrating the conditional quantities with the filtered probability density function $\widetilde{P}(\eta)$ as follows:

$$\widetilde{f} = \int_0^1 \widetilde{f|\eta}\;\widetilde{P}(\eta)\,d\eta \tag{8}$$

where $\widetilde{P}(\eta)$ is given as a β-function, which is obtained using the resolved mixture fraction $\widetilde{\xi}$ and its sub-grid scale variance $\widetilde{\xi''^2}$. More details concerning the coupling between LES and CMC are given in Ref. (Foale 2022; Awad et al. 2025b).

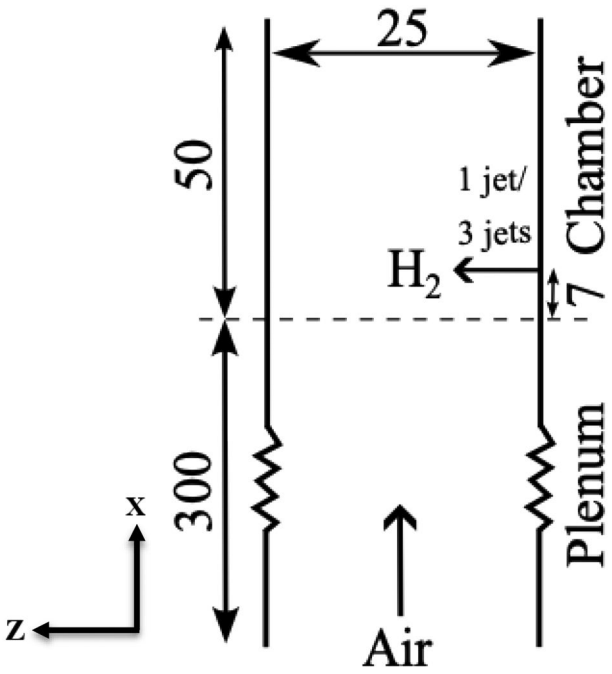

Fig. 1 Schematic of the simulated burner configuration (Rajendram Soundararajan et al. 2025)

Table 1 Operating conditions for all cases investigated

Case	U_∞ (m/s)	U_j (m/s)	J	$\frac{\rho_j}{\rho_\infty}$	Re_j
Non-reacting-He	2.8	161	462	0.14	6.7×10^2
Non-reacting-H2	2.8	226	462	0.07	1.0×10^3
Reacting	3.7	226	260	0.07	1.0×10^3

2.2 Simulated Burner Configuration

The simulation is based on the JICF burner configuration investigated by Rajendram Soundararajan et al. (2025). The cold-side section through which air flows is formed by a 300 mm long square cross-section channel followed by optically-accessible combustion chamber that houses the flame. The chamber is formed by three quartz walls of 50 mm in height and a metal plate on the fourth side on which the hydrogen jets are located at 7 mm above the chamber inlet. A schematic of the burner is shown in Fig. 1. The hydrogen injection plate consists of either three injection holes separated by a distance of 5 mm or a single injection hole with 0.5 mm diameter (i.e., $d = 0.5$ mm). The inlet air and fuel temperature are 300 K, and the operating pressure is 1 atm. During the non-reacting JICF and MJICF experiments, hydrogen was replaced by helium for safety reasons, but the momentum flux ratios were matched to that of hydrogen. Thus, in the current study, an assessment of the use of helium instead of hydrogen for cold flow experiments will also be investigated. The investigated conditions for reacting and non-reacting simulations are shown in Table 1. The jet Reynolds numbers are Re $\approx 6.7 \times 10^2$ for He and Re $\approx 1.0 \times 10^3$ for H_2, corresponding to a transitional regime. These values indicate the presence of unsteady shear-layer instabilities

and the onset of turbulence, which are essential to the flame stabilization and mixing mechanisms in jets in crossflow. The corresponding Mach numbers remain modest (M ≈ 0.16–0.8), confirming that compressibility effects are negligible. The transitional Reynolds numbers and inherently unsteady shear-layer dynamics justify the use of LES, which can accurately resolve the large-scale vortex structures and mixing processes that cannot be captured by steady RANS approaches.

2.3 Numerical Implementation

The numerical simulations are conducted using the Rolls-Royce in-house code PRECISE-UNS (Anand et al. 2013; Awad et al. 2025c, d). PRECISE-UNS is coupled with the code CLIO (Awad et al. 2025b; Giusti and Mastorakos 2017; Gkantonas et al. 2020) for the solution of the CMC equations, which are solved using the operator splitting method. The CMC terms in physical space are solved first, with a first-order upwind scheme for the transport in physical space and a first-order Euler scheme for temporal discretisation. This is followed by the solution of the micromixing terms using the TDMA method and finally, the chemical source term is evaluated using the SpeedCHEM package (Perini et al. 2012). A chemical mechanism, which consists of 10 species and 31 reactions, has been employed for hydrogen chemistry (Hong et al. 2011). For the boundary conditions on the CMC level, an inert mixing solution is used at the inlet, whereas a zero-gradient boundary condition is used at the outlet and the walls. CMC cells are initialised using a fully burning distribution obtained using a stand-alone 0D-CMC code, where the multi-dimensional form of the CMC equations is solved without the transport terms in physical space. On the LES level, a first-order Euler scheme has been employed for the time derivatives and a second-order accuracy scheme has been used for the spatial discretization. For the boundary conditions on the LES level, inflow boundary condition with a uniform velocity profile is imposed at the air and fuel inlet with no synthetic turbulent imposed. A pressure outlet is applied at the burner exit and no-slip boundary conditions have been imposed at the walls. The unconditional filtered quantities are evaluated from the conditional quantities using the filtered probability density function, which is modelled using a β-function. Mixture fraction space is discretised using 51 nodes refined near the stoichiometric ξ for hydrogen (i.e., ξ_{st}=0.028). The LES mesh consists of about 4 M tetrahedral cells, whereas the CMC mesh consists of about 10 K polyhedral cells refined near the jet inlet and the expected flame location from the experiment. The LES mesh resolves more than 80% of the turbulent kinetic energy fulfilling Pope's criterion for LES (Pope 2004). Moreover, the ratio between the grid resolution relative to the Kolmogorov length scale falls within a range of 15 to 30, indicating a well-resolved LES mesh. The local grid spacing near the injector is sufficiently small relative to the jet diameter to capture the main shear-layer dynamics and jet–crossflow interaction. The near-wall resolution corresponds to y+≈3–5, which is adequate to capture the boundary-layer behaviour.

3 Results and Discussion

3.1 Non-Reacting (Helium vs. Hydrogen)

Figure 2 shows a comparison between the instantaneous experimental and numerical Schlieren images for helium (He) and hydrogen (H2) non-reacting jets under the same momentum flux ratio. The numerical Schlieren is approximated using the density gradient (i.e., $\approx |\nabla \rho|$), and the comparison with the experimental data is obtained by averaging various planes in the spanwise direction (i.e., y direction). Reasonable agreement between the experimental and numerical schlieren is observed for the helium case, with a reasonable prediction for the jet penetration depth (i.e., jet stem). On comparing the helium and hydrogen cases, considerable differences between helium and hydrogen in terms of the jet stem and the vortical structures downstream of the jet exit can be observed. Moreover, the hydrogen case exhibits small H_2 structures near the opposite wall, which is not observed for the helium case. To explain the appearance of the small H_2 structures near the opposite wall, the H_2 mass fraction at a plane located near the centreline is shown in Fig. 3. It can be observed that these H_2 structures originate from a weak corner recirculation that carries trace amounts of H_2 downstream of the main jet. This behaviour arises from H_2's higher diffusivity and lower density, which enhance lateral spreading and entrainment compared to He. The corresponding velocity field shows no upstream motion, confirming that there is no reverse H_2 transport. The small variations in H_2 concentration significantly alter the local density and these recirculated H_2 pockets generate weak density gradients that become visible in the line-of-sight numerical Schlieren images shown in Fig. 2.

The vortex structures for both hydrogen and helium can be visualised using the Q-criterion. Figure 4 shows an iso-surface of the Q-criterion coloured by the vorticity vector in the streamwise direction (i.e., x direction). It can be observed that both cases show the typical JICF topologies such as the CVPs, which can be observed with rotating vortices of opposite signs, and the SLVs, which are observed on both the leeward and windward sides of the

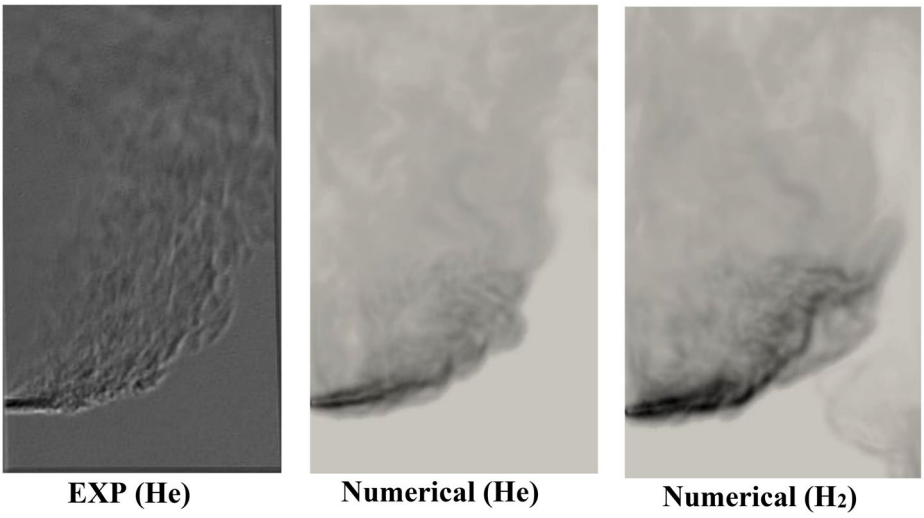

Fig. 2 Experimental vs. numerical schlieren

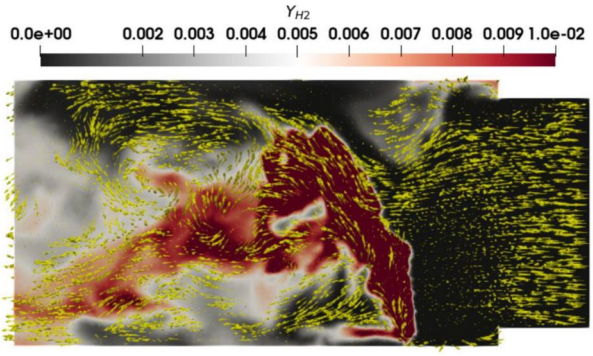

Fig. 3 H2 mass fraction at a plane located near the burner centre line. Yellow: streamwise velocity component

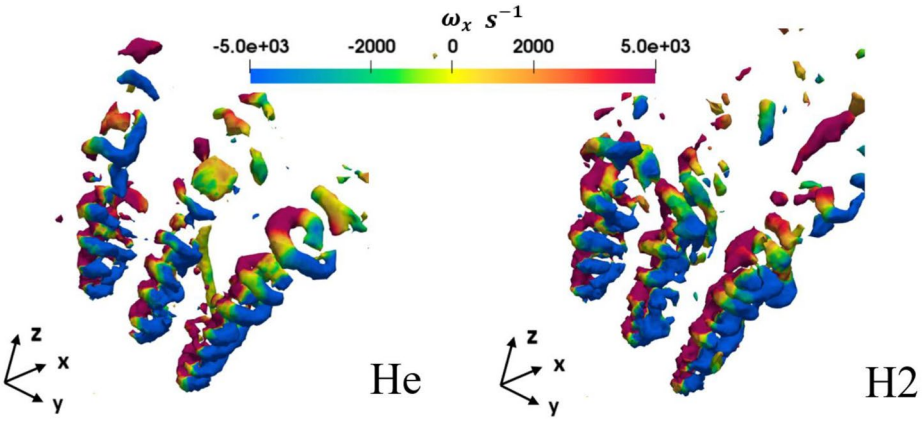

Fig. 4 Iso-surface of the Q-criterion at Q=9 $\times 10^6$ coloured by the vorticity vector in the streamwise direction (i.e., x direction) for both helium (left) and hydrogen (right)

jet. However, SLVs are less distinct for the hydrogen case compared to the helium case. To provide a quantitative description of the mixing and assess the mixing properties for both hydrogen and helium, the spatial mixing deficiency (SMD) and temporal mixing deficiency (TMD) are investigated. The TMD represents the temporal heterogeneity of the mixture, whereas the SMD indicates the spatial heterogeneity of the mixture at various locations downstream of the jet exit. The SMD and TMD are defined as in (Priere et al. 2004):

$$\mathrm{SMD} = \frac{\sqrt{\frac{1}{m-1}\sum_{i=1}^{m}\left[\left(\bar{Y}_{fi} - \langle \bar{Y}_{fi}\rangle_{plane}\right)\right]^2}}{\langle \bar{Y}_{fi}\rangle_{plane}} \tag{9}$$

$$\mathrm{TMD} = \frac{1}{m}\sum_{i=1}^{m}\left(\frac{Y_{rms_i}}{\bar{Y}_{fi}}\right) \tag{10}$$

where $\bar{Y}_{fi}$ and Y_{rms_i} are the mean and root mean square mass fraction of helium or hydrogen at cell i. $\langle \bar{Y}_{fi} \rangle_{\text{plane}}$ is the mean mass fraction on a given plane (i.e., $\langle \bar{Y}_{fi} \rangle_{\text{plane}} = \frac{1}{m} \sum_{i=1}^{m} \bar{Y}_{fi}$) and m is the number of cells. A zero SMD or TMD indicates a perfect mixing scenario, whereas, as the value increases the departure from a perfect mixing increases. Figure 5 shows the SMD and TMD at various planes downstream of the jet exit (i.e., x=0) for both helium and hydrogen under the same momentum flux ratio. In the Q-criterion visualization, the hydrogen case shows less distinct SLVs than helium. Consistent with this observation, hydrogen exhibits enhanced mixing relative to helium, as quantified by its lower SMD and TMD values at all downstream locations from the jets. It can also be seen from Fig. 5 that both mixing indices decrease considerably further downstream for both gases. However, hydrogen has a faster jet-decay rate compared to helium. The lower SMD and TMD for hydrogen therefore indicate a more homogeneous mixing field compared to helium.

3.2 Flame Stabilisation Mechanism

Figure 6 shows a comparison between the experimental average OH* chemiluminescence and the mean heat release rate (HRR) in the front view (i.e., facing the three jets) and the side view of the burner. The comparison with the experimental data is obtained by averaging the mean heat release rate from the simulations on various planes in the line-of-sight direction (i.e., y-direction for Fig. 6a and z-direction for Fig. 6b). Reasonable agreement between the experiment and numerical simulation is observed in terms of the overall flame shape. However, an underprediction for the jet stem is observed compared to the experimental data. Moreover, some discrepancies are observed in the predicted flame tip. Given the adequately resolved LES mesh near the wall and jet exit, the discrepancy in the observed flame tip might be attributed to the CMC mesh resolution as the size of local extinction remains sensitive the CMC resolution (Garmory and Mastorakos 2015) as each CMC cell represents an ensemble of LES cells from which conditional quantities such as the scalar-dissipation rate are averaged. However, it is worth noting that the CMC grid considered in this analysis is fine by typical LES-CMC standards. Figure 7 shows the instantaneous temperature field,

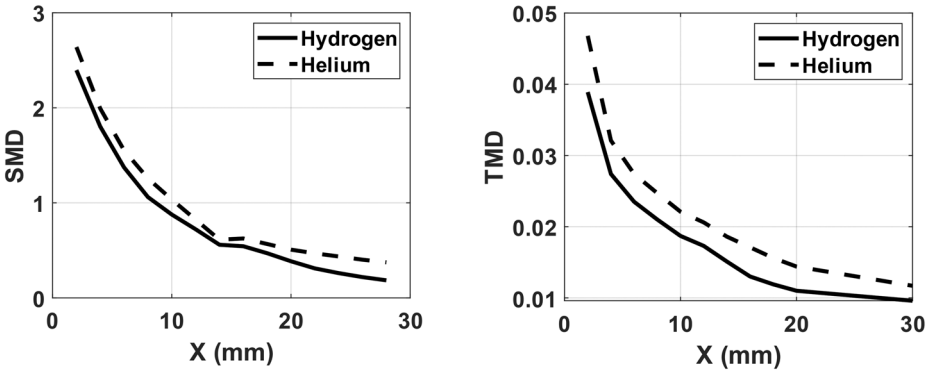

Fig. 5 SMD and TMD vs. distance in the streamwise direction

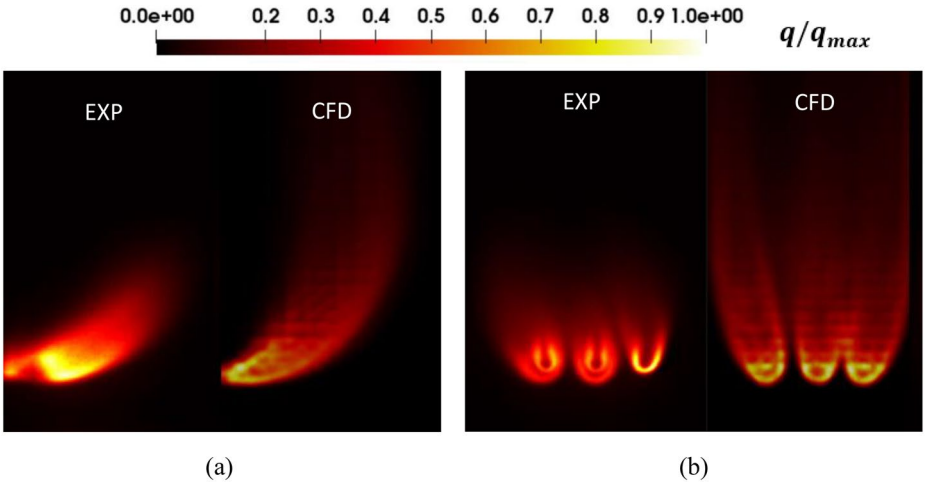

Fig. 6 Experimental average OH* chemiluminescence intensity vs. mean HRR from the CFD. A side view is shown on the left and a front view on the right. q/q_{max} is the normalised mean HRR in the CFD or the OH* intensity in the experiments

mean temperature field and the mean streamwise velocity for both SJICF and MJICF under the same momentum flux ratio at the mid-z-x plane. And the mean temperature at a plane located normal to the jet exit is shown in Fig. 8. It can be clearly observed from the mean streamwise velocity field that flame stabilisation is achieved through the recirculation zone in the jet wake, which provides the mixing of the hot products of combustion with the fresh reactants thereby sustaining the flame.

Moreover, it can be observed that the LES resolves the Kelvin-Helmholtz instability, as evidenced by wave-like behaviour on the windward side of the flame for both SJICF and MJICF. In terms of the flame lift-off high, which is here determined based on the flame location corresponding to a peak mean temperature of 900 K following (Kim and Mastorakos 2005; Cheng et al. 1992), it can be observed from the mean temperature field for the MJICF that the flame remains attached to the leeward side and slightly lifted on the windward side. However, the SJICF reveal a slightly lifted flame on both the leeward and windward sides. The slight windward side lift-off height for MJICF can be clearly observed in Figs. 9 and 10, which shows differences in the conditionally filtered temperature and species mass fractions (H2O, OH and HO2) for the locations (P1, P2 & P3) given in Fig. 7.

It can further be observed from Fig. 7 that SJICF has higher penetration depth into the cross-flow compared to the MJICF case. This behaviour could be attributed to the proximity of the CVPs of the three jets, which induces negative radial velocity components that influence the jet penetration depth. This can further be confirmed using the probability density function (PDF) of the mean z-velocity component extracted throughout the whole domain, which indicates a higher probability of finding negative velocities for MJICF compared to SJICF (Fig. 11). This behaviour is not caused by additional flow blockage due to the larger frontal area of the MJICF configuration. As shown in Fig. 12, the mean streamwise velocity

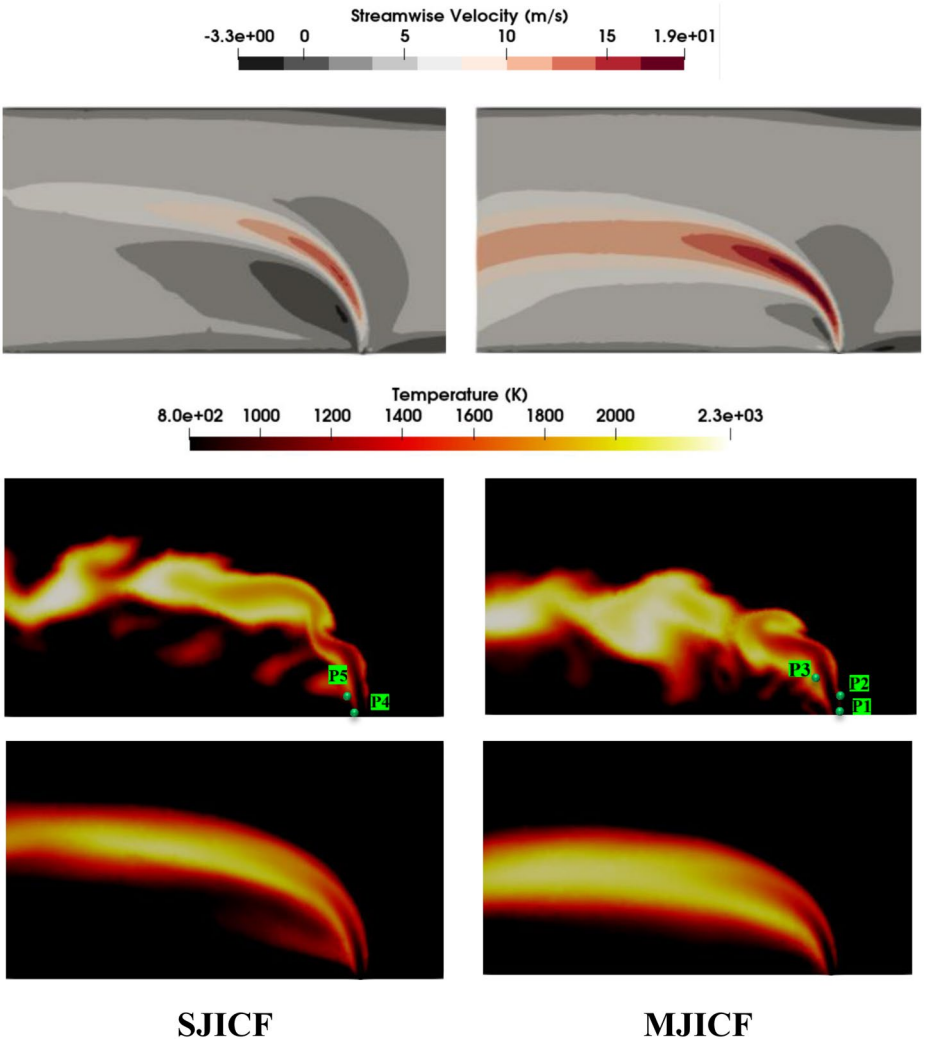

Fig. 7 Mean streamwise velocity component (top), instantaneous temperature field (middle), and mean temperature field (bottom) at the centre line for both SJICF (left) and MJICF (right)

at a plane just upstream of the jets is not significantly different for both SJICF and MJICF. The plane-averaged mean streamwise velocity differs by less than 0.1%, confirming that the bulk cross-flow is not accelerated and that the reduced jet penetration observed in MJICF cannot be attributed to blockage effects and mainly due to the induced negative z velocity components. To further verify that this behaviour is also not influenced by reacting effects, a complementary cold-flow analysis was performed. Figure 13 presents the instantaneous mixture fraction and the mean z velocity component on a representative y-z plane down-

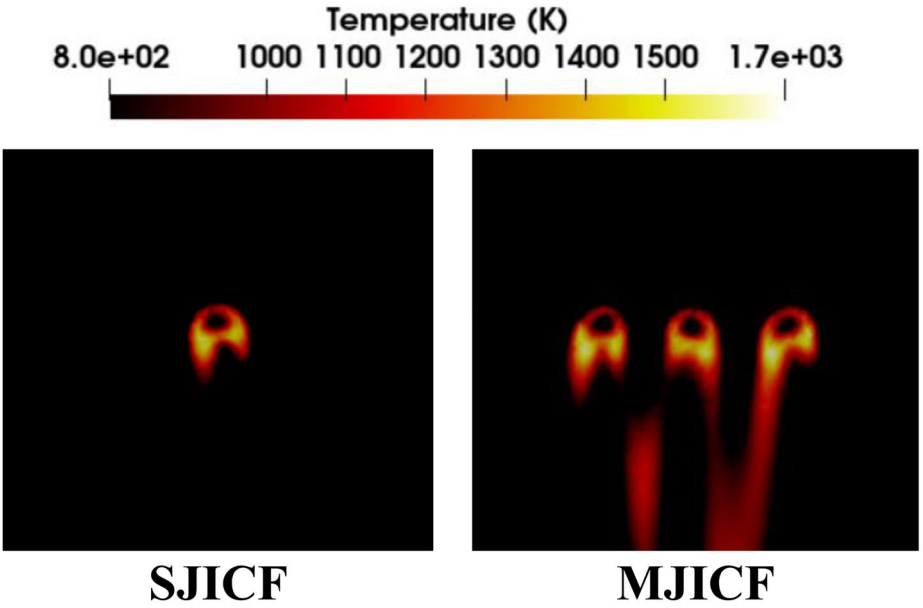

Fig. 8 Mean temperature field at plane normal to the jet exit

stream of the injector array. The cold-flow results exhibit the same trend observed under reacting conditions: the SJICF shows a higher jet penetration depth, while the MJICF develops stronger regions of negative z velocity associated with the interaction and merging of adjacent CVPs. In contrast, the SJICF displays weaker negative z velocity, consistent with its greater penetration depth.

To investigate the flame stabilisation mechanism, the budget of the CMC equation terms is investigated at two locations for both SJICF and MJICF. For the sake of convenience, the Q_{H2O} equation is recalled here for readability:

$$\frac{\partial Q_{H2O}}{\partial t} = \underbrace{-\frac{\partial}{\partial x_i}\left(Q_{H2O}\ \widetilde{u_i|\eta}\right)}_{T1} + \underbrace{Q_{H2O}\frac{\partial}{\partial x_i}\left(\widetilde{u_i|\eta}\right)}_{T2} + \underbrace{\widetilde{N|\eta}\ \frac{\partial^2 Q_{H2O}}{\partial \eta^2}}_{T3} + \underbrace{\widetilde{\dot{\omega}_{H2O}|\eta}}_{T4} + \underbrace{e_{H2O}}_{T5} \quad (11)$$

The budget analysis of the conditional H_2O transport equation explicitly quantifies how the dominant physical processes vary across mixture-fraction space and at different positions relative to the stabilization point. Thus, the influence of mixture fraction on the stabilization mechanism is directly captured through the CMC budgets. It is worth noting that while CMC with mixture fraction conditioning is formulated for non-premixed flames, it can still provide insights into premixed behaviour through specific budget signatures. In CMC, with the mixture fraction as the conditional variable, the effects of premixed flame propagation are captured within the conditional turbulent flux term (i.e., T5). This term accounts for fluctuations arising from deviations from the standard mixture fraction-state relationship, which occur due to premixed combustion behaviour. The budget balance we observe—

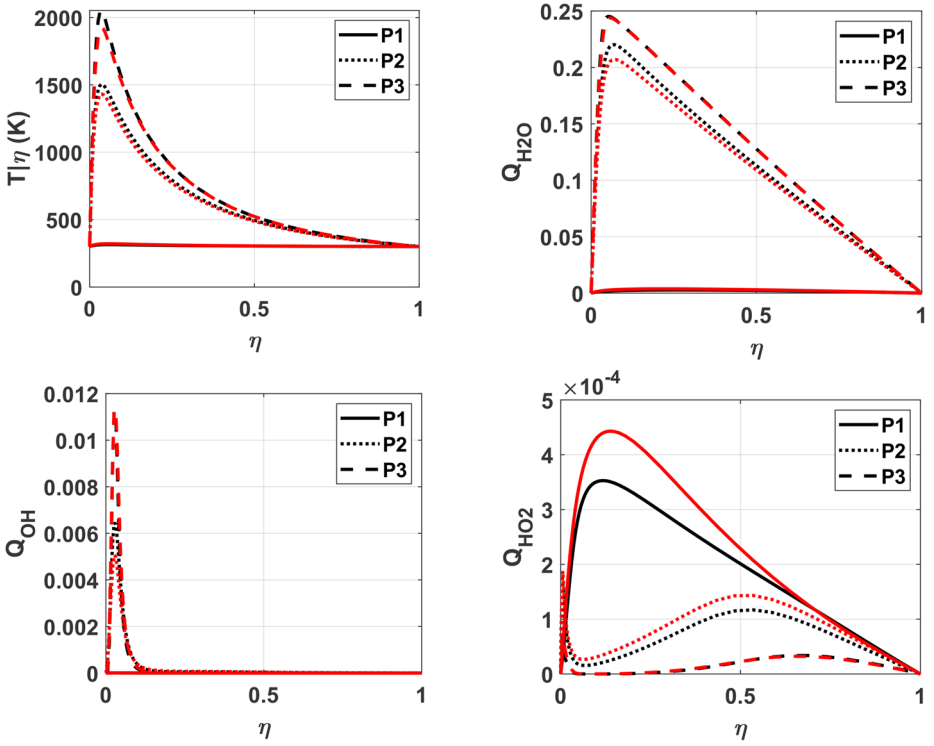

Fig. 9 The conditional temperature and some major and minor species at locations P1, P2 and P3 (see Fig. 7) for MJICF at 1.7 (black) and 2 (red) flow through time

where convection and turbulent diffusion dominate while the molecular dissipation term remains negligible—can be considered as a signature of premixed flame stabilization in the CMC context. The shift in balance from reaction-micromixing to convection-turbulent diffusion indicates that flame propagation, rather than non-premixed, governs the stabilization mechanism. This interpretation is consistent with previous studies (Patwardhan et al. 2009; Navarro-Martinez and Kronenburg 2011) that identified similar budget shifts as indicators of premixed combustion behaviour within CMC frameworks. The budge analysis is investigated at two location P4 and P5 (see Fig. 6). The first location is located just upstream of the reactive zone, whereas the second location lies further downstream (i.e., inside the reactive zone). It can be seen from Figs. 14 and 15 that upstream the reactive zone the chemical (i.e., T4) and micromixing terms (i.e., T3) have negligible values and a balance between the convection term (i.e., T1 + T2) and the turbulent diffusion term (i.e., T5) is observed. This, in turn, suggests that the flame structure is close to a premixed flame behaviour (i.e., the preheat zone of a premixed flame has a convection-diffusion balance). This behaviour remains consistent with the budget of CMC terms in lifted turbulent jet flames, where the turbulent premixed flame structure is also observed upstream of the reactive zone (Patward-

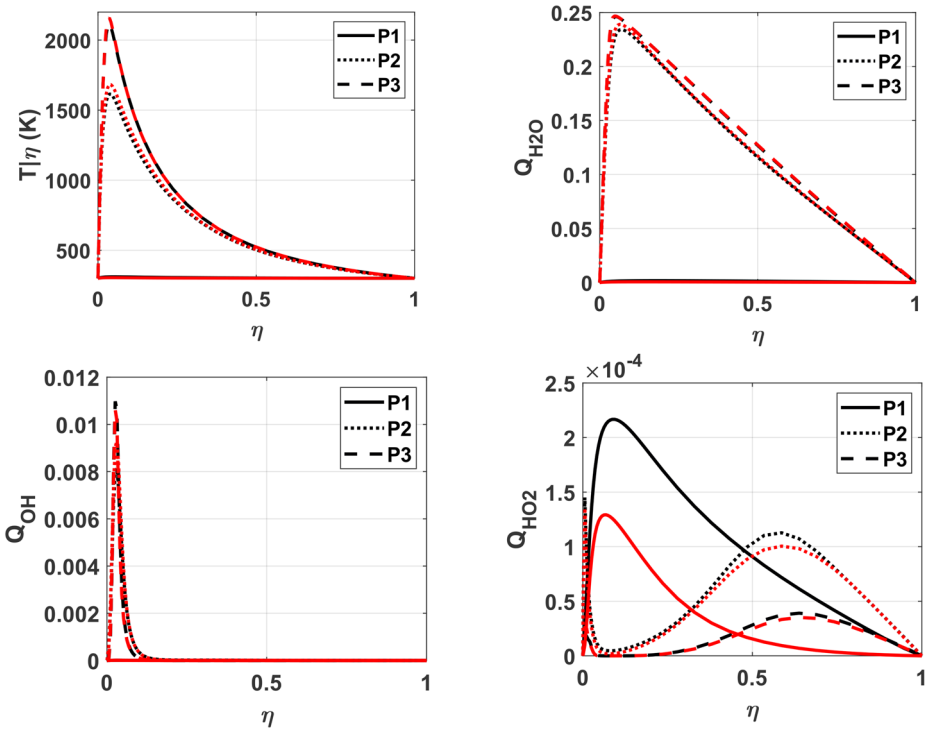

Fig. 10 The conditional temperature and some major and minor species at locations P1, P2 and P3 (see Fig. 7) for SJICF at 1.7 (black) and 2 (red) flow through time

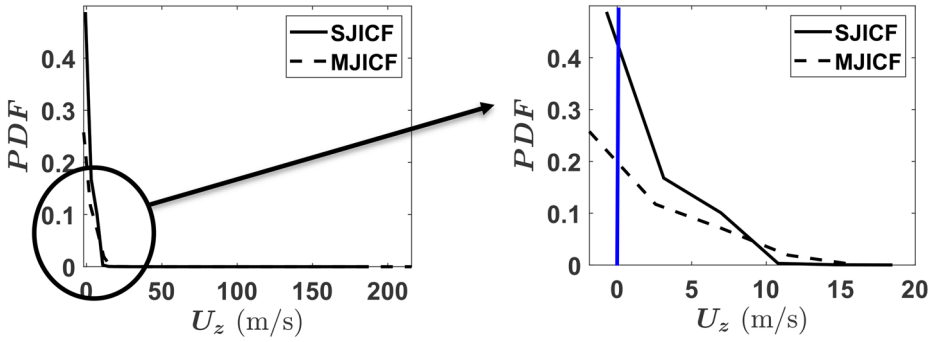

Fig. 11 PDF of the z-velocity component for SJICF and MJICF extracted over the whole domain at 1.7 flow through time

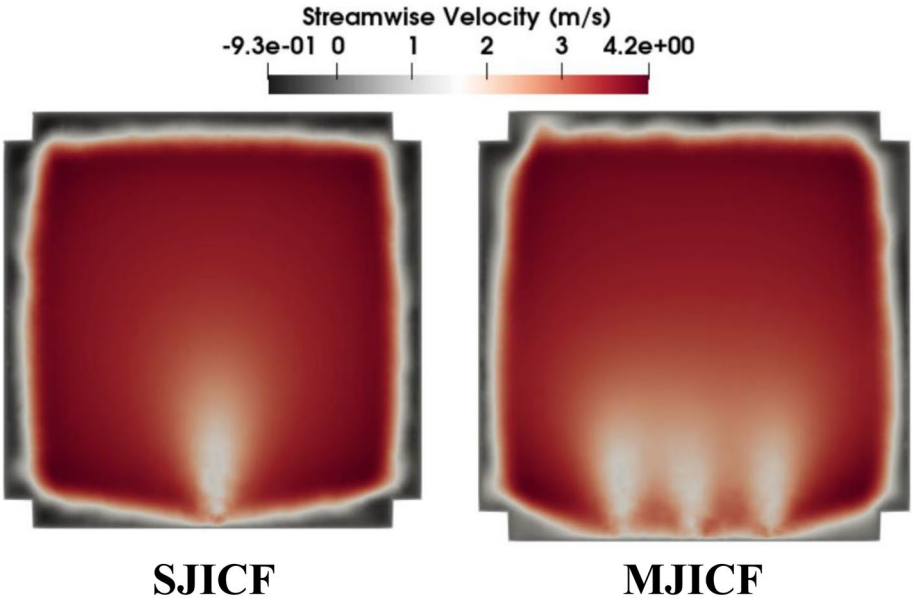

Fig. 12 Mean streamwise velocity component at a plane just upstream of the jets

han et al. 2009). It can be further observed from Fig. 10 that MJICF has a higher magnitude of the convective term compared to SJICF, whereas the turbulent diffusion term remains comparable for both cases. Moreover, at the reactive zone, a principle balance between the micromixing term and the chemical term is observed for both SJICF and MJICF. This suggests that the flame attains the behaviour of a non-premixed flame structure.

4 Conclusion

Large eddy simulation (LES) with the Conditional Moment Closure (CMC) has been used to investigate the flame stabilisation mechanism in reacting single and multiple jets in a cross-flow configuration. The analysis was conducted for pure hydrogen with chemical kinetics comprising 10 species and 31 reactions, and the results were compared against corresponding experiments. Cold-flow experiments have been performed using helium instead of hydrogen for safety reasons. Thus, before initiating the reacting simulations, a non-reacting LES investigation has been performed to illustrate the differences between helium and hydrogen.

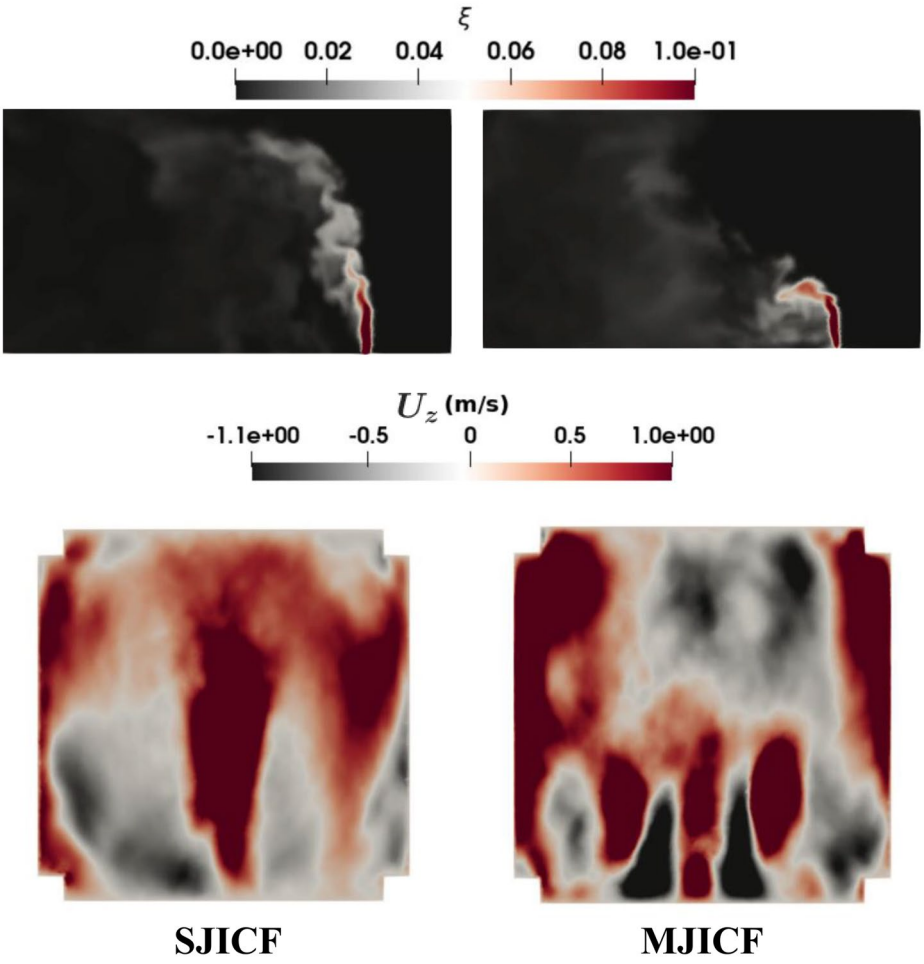

Fig. 13 Instantaneous mixture fraction (top) and the mean vertical velocity component on a representative y-z plane downstream of the injector array (bottom)

The main findings of the present research are as follows:

1) Differences between helium and hydrogen are observed in terms of the jet stem and the vortical structures, with better air-fuel mixing achieved for hydrogen.
2) MJICF has a shorter jet stem compared to SJICF due to the proximity of the CVPs of the three jets, which induce negative velocity components towards the jet exit thereby influencing the jet stem.
3) The analysis of the CMC equation budget reveals that upstream of the reactive zone, the flame reveals a premixed flame structure with a convection-diffusion balance. However, further downstream, non-premixed combustion is observed with a balance between the chemical term and the micromixing term.

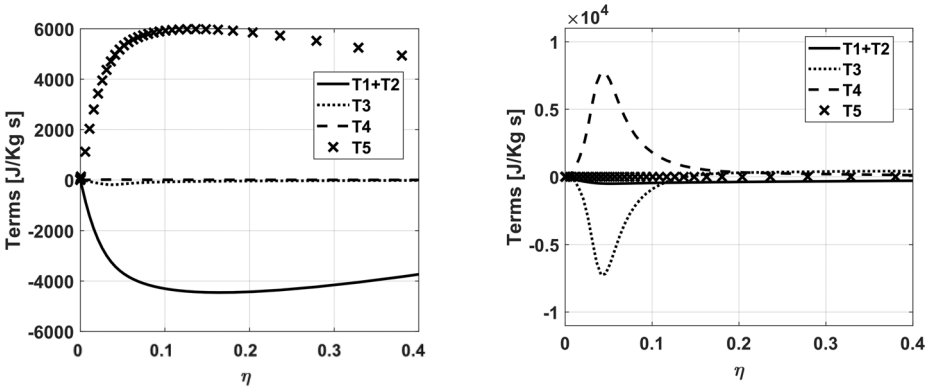

Fig. 14 Budget of CMC terms for the conditional H2O transport equation upstream of the stabilisation location (left P4) and downstream of the stabilisation location (right P5) for SJICF at 1.7 flow through times

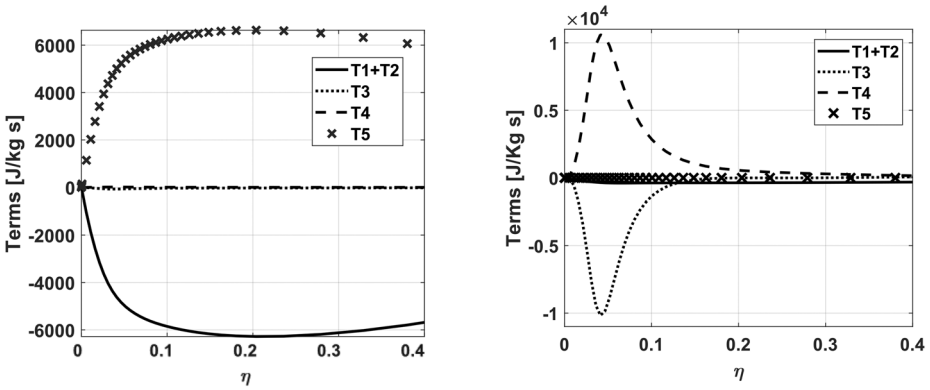

Fig. 15 Budget of CMC terms for the conditional H2O transport equation upstream of the stabilisation location (left P4) and downstream of the stabilisation location (right P5) for MJICF at 1.7 flow through times

Acknowledgements We acknowledge funding from the UKRI under the Horizon Europe Guarantee (European Union Horizon 2020 Research and Innovation Program project HESTIA, EU grant agreement no. 101056865, UKRI agreement 10042258). The simulations were performed on the Cambridge Service for Data Driven Discovery (CSD3) supercomputer.

Author Contributions H.A.: writing—original draft, visualisation, software, methodology, investigation, formal analysis, data curation, and conceptualisation. S.G.: software, visualisation, methodology, investigation and formal analysis. P.R: writing—review and editing, visualisation, methodology, investigation and formal analysis. E.M.: writing—review and editing, supervision, resources, funding acquisition, and conceptualisation.

Funding We acknowledge funding from the UKRI under the Horizon Europe Guarantee (European Union Horizon 2020 Research and Innovation Program project HESTIA, EU grant agreement no. 101056865, UKRI agreement 10042258).

Data Availability Data will be available on request.

Declarations

Ethical Approval No specific ethical approval is required for this work.

Informed Consent Not applicable for this work.

Competing Interests The authors declare no competing interests.

References

Abo-Amsha, K., Awad, H.S.A.M., Chakraborty, N.: Flame self-interactions in MILD combustion of homogeneous and inhomogeneous mixtures. Sci. Rep. **14**(1), 5525 (2024)

Anand, M.S., Eggels, R.L.G.M., Staufer, M., Zedda, M., Zhu, J.: An advanced unstructured-grid finite-volume design system for gas turbine combustion analysis. In Gas Turbine India Conference ASME. **35161**, Paper No. V001T03A003 (2013)

Awad, H.S., Gkantonas, S., Mastorakos, E., Eggels, R.: Parametric analysis of hydrogen swirl combustors with incompletely stirred reactor network modelling. J. Propuls. Power. (2025a). https://doi.org/10.2514/1.B40190

Awad, H.S., Gkantonas, S., Mastorakos, E.: A spark energy deposition model in mixture fraction space for simulations of turbulent Non-Premixed flame ignition. Appl. Energy Combust. Sci. **21**, 100317 (2025b)

Awad, H.S., Gkantonas, S., Mastorakos, E.: Low-Order modelling of extinction of hydrogen Non-Premixed swirl flames. Aerospace. **12**(8), 676 (2025c)

Awad, H., Mesquita, L., Stow, S., Mastorakos, E.: Predicting the ignition loop in realistic combustors at high altitude conditions. AIAA SCITECH Forum, 1331 (2025d)

Bilger, R.W.: Conditional moment closure for turbulent reacting flow. Phys. Fluids A. **5**(2), 436–444 (1993)

Chan, W.L., Ihme, M.: Large-Eddy simulation of a turbulent reacting jet in crossflow. Proceedings of the 8th US National Combustion Meeting. Paper No. 070LT-0108 (2013)

Chen, J.H., Echekki, T., Kollmann, W.: The mechanism of two-dimensional pocket formation in lean premixed methane-air flames with implications to turbulent combustion. Comb. Flame. **116**(1–2), 15–48 (1999)

Cheng, T.S., Wehrmeyer, J.A., Pitz, R.W.: Simultaneous temperature and multispecies measurement in a lifted hydrogen diffusion flame. Comb. Flame. **91**(3–4), 323–345 (1992)

Foale, J.M.: Simulating extinction and blow-off in kerosene swirl spray. PhD thesis, University of Cambridge (2022)

Garmory, A., Mastorakos, E.: Numerical simulation of oxy-fuel jet flames using unstructured LES–CMC. Proc. Comb. Inst. **35**(2), 1207–1214 (2015)

Giusti, A., Mastorakos, E.: Detailed chemistry LES/CMC simulation of a swirling ethanol spray flame approaching blow-off. Proc. Combust. Inst. **36**(2), 2625–2632 (2017)

Gkantonas, S., Mastorakos, E.: Low-Order autoignition modeling for hydrogen transverse jets. J. Propul. Power. **39**(5), 728–742 (2023)

Gkantonas, S., Sirignano, M., Giusti, A., D'Anna, A., and Mastorakos, E.: Comprehensive soot particle size distribution modelling of a model Rich-Quench-Lean burner. Fuel. **270**, 117483 (2020)

Grout, R.W., Gruber, A., Yoo, C.S., Chen, J.H.: Direct numerical simulation of flame stabilization downstream of a transverse fuel jet in cross-flow. Proc. Comb. Inst. **33**(1), 1629–1637 (2011)

Grout, R.W., Gruber, A., Kolla, H., Bremer, P.T., Bennett, J.C., Gyulassy, A., Chen, J.H.: A direct numerical simulation study of turbulence and flame structure in transverse jets analysed in jet-trajectory based coordinates. J. Fluid Mech. **706**, 351–383 (2012)

Hasselbrink, E.F. Jr., Mungal, M.G.: Observations on the stabilization region of lifted non-premixed methane transverse jet flames. In Symposium (International) on combustion. **27**(1), 1167–1173 (1996)
Hong, Z., Davidson, D.F., Hanson, R.K.: An improved H2/O2 mechanism based on recent shock tube/laser absorption measurements. Comb. Flame. **158**(4), 633–644 (2011)
Huang, R.F., Wang, S.M.: Characteristic flow modes of wake-stabilized jet flames in a transverse air stream. Comb. Flame. **117**(1–2), 59–77 (1999)
Im, H.G., Chen, J.H.: Preferential diffusion effects on the burning rate of interacting turbulent premixed hydrogen-air flames. Comb. Flame. **131**(3), 246–258 (2002)
Kadota, T., Wang, J.X., Kawaoka, T.: Structure of propane jet diffusion flame in a cross flow. JSME Int. J. Ser. **2**(3), 575–581 (1990). Fluids Engineering, Heat Transfer, Power, Combustion, Thermophysical Properties
Kamotani, Y., Greber, I.: Experiments on confined turbulent jets in cross flow. 6th Fluid and Plasma Dynamics Conference. **647** (1974)
Karagozian, A.R.: Transverse jets and their control. Prog Energy Comb. Sci. **36**(5), 531–553 (2010)
Kelso, R.M., Lim, T., Perry, A.: An experimental study of round jets in cross-flow. J. Fluid Mech. **306**, 111–144 (1996)
Kim, I.S., Mastorakos, E.: Simulations of turbulent lifted jet flames with two-dimensional conditional moment closure. Proc. Comb. Inst. **30**(1), 911–918 (2005)
Klimenko, A.Y.: Multicomponent diffusion of various admixtures in turbulent flow. Fluid Dyn. **25**(3), 327–334 (1990)
Klimenko, A.Y., Bilger, R.W.: Conditional moment closure for turbulent combustion. Prog Energy Comb. Sci. **25**(6), 595–687 (1999)
Kolla, H., Grout, R.W., Gruber, A., Chen, J.H.: Mechanisms of flame stabilization and blowout in a reacting turbulent hydrogen jet in cross-flow. Comb. Flame. **159**(8), 2755–2766 (2012)
Muralidharan, B., Menon, S.: Large eddy simulation of turbulent reacting jet in cross flow with adaptive mesh refinement. 52nd Aero. Sci. Meet. Paper No. 0825 (2014)
Navarro-Martinez, S., and Kronenburg, A.: Flame stabilization mechanisms in lifted flames. Flow. Turb. Comb. **87**(2), 377–406 (2011)
O'Brien, E.E., Jiang, T.L.: The conditional dissipation rate of an initially binary scalar in homogeneous turbulence. Phys. Fluids A. **3**(12), 3121–3123 (1991)
Patwardhan, S.S., De, S., Lakshmisha, K.N., Raghunandan, B.N.: CMC simulations of lifted turbulent jet flame in a vitiated coflow. Proc. Comb. Inst. **32**(2), 1705–1712 (2009)
Perini, F., Galligani, E., Reitz, R.D.: An analytical Jacobian approach to sparse reaction kinetic for computationally efficient combustion modeling with large reaction mechanisms. Energy Fuels. **26**(8), 4804–4822 (2012)
Pope, S.B.: Ten questions concerning the large-eddy simulation of turbulent flows. New J. Phys. **6**(1), 35 (2004)
Priere, C., Gicquel, L.Y.M., Kaufmann, P., Krebs, W., Poinsot, T.: Large eddy simulation predictions of mixing enhancement for jets in cross-flows. J. Turbul. **5**(1), 005 (2004)
Saini, P., Chterev, I., Pareja, J., Aigner, M., Boxx, I.: Effects of hydrogen-enrichment on flameholding of natural gas jet flames in crossflow at elevated temperature and pressure. Flow. Turb Comb. **107**(1), 219–243 (2021)
Soundararajan, P.R., Gauthier, P.Q., Benie, P.J., Mastorakos, E.: A joint experimental and numerical study of multiple hydrogen flames in a jet in crossflow configuration. Proc. Comb. Inst. **41**, 105929 (2025)
Steinberg, A.M., Sadanandan, R., Dem, C., Kutne, P., Meier, W.: Structure and stabilization of hydrogen jet flames in cross-flows. Proc. Comb. Inst. **34**(1), 1499–1507 (2013)
Yao, Y., Petty, D., Barrington, P., Yao, J., Mason, P.: Direct numerical simulation of jets in cross-flow. Int. J. Comput. Fluid Dyn. **20**(5), 279–285 (2006)
Zhang, H., Mastorakos, E.: Prediction of global extinction conditions and dynamics in swirling non-premixed flames using LES/CMC modelling. Flow, turb. Comb. **96**(4), 863–889 (2016)
Zhang, H., Garmory, A., Cavaliere, D.E., Mastorakos, E.: Large eddy simulation/conditional moment closure modeling of swirl-stabilized non-premixed flames with local extinction. Proc. Comb. Inst. **35**(2), 1167–1174 (2015)